


FULL ARTICLE

easySLM-STED: Stimulated emission depletion microscopy with aberration correction, extended field of view and multiple beam scanning

Frederik Görlitz^{1*}  | Stina Guldbbrand¹ | Timothy H. Runcorn² | Robert T. Murray² | Angel L. Jaso-Tamame³ | Hugo G. Sinclair¹ | Enrique Martinez-Perez³ | James R. Taylor² | Mark A. A. Neil¹ | Christopher Dunsby^{1,4} | Paul M. W. French^{1*}

¹Photonics Group, Department of Physics, Imperial College London, London, UK

²Femtosecond Optics Group, Department of Physics, Imperial College London, London, UK

³London Institute of Medical Sciences, Imperial College London, London, UK

⁴Centre for Pathology, Imperial College London, London, UK

*Correspondence

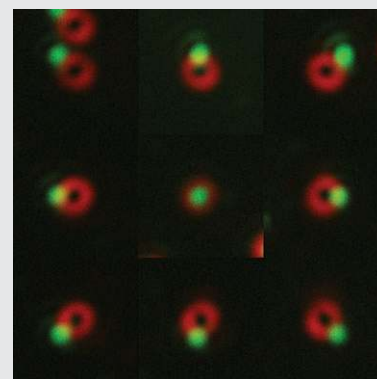
Paul M. W. French, Photonics Group, Department of Physics, Imperial College London, London SW7 2BB, UK.

Email: paul.french@imperial.ac.uk
Frederik Görlitz, Photonics Group, Department of Physics, Imperial College London, London SW7 2BB, UK.
Email: f.gorlitz14@imperial.ac.uk

Funding information

Engineering and Physical Sciences Research Council; Medical Research Council, Grant/Award Number: MR/K015834/1

We demonstrate a simplified set-up for STED microscopy with a straightforward alignment procedure that uses a single spatial light modulator (SLM) with collinear incident excitation and depletion beams to provide phase modulation of the beam profiles and correction of optical aberrations. We show that this approach can be used to extend the field of view for STED microscopy by correcting chromatic aberration that otherwise leads to walk-off between the focused excitation and depletion beams. We further show how this arrangement can be adapted to increase the imaging speed through multibeam excitation and depletion. Fine adjustments to the alignment can be accomplished using the SLM only, conferring the potential for automation.



KEYWORDS

aberration correction, spatial light modulator, STED, super resolved microscopy

1 | INTRODUCTION

Laser scanning confocal microscopy (LSCM) is a ubiquitous tool to provide diffraction-limited optically sectioned images and is widely applied to image fluorescent biological samples. Stimulated emission depletion (STED) microscopy [1, 2] is a development of LSCM that overcomes the diffraction limit by utilizing reversible photoswitching of the fluorophore emission such that the detected fluorescence photons

originate from a region that can be arbitrarily small. As such, STED microscopy is a member of the “RESOLFT” [3] class of super-resolved microscopy (SRM) techniques. In STED microscopy, the fluorescence emission in a LSCM is spatially modulated by depletion of the excited state population through stimulated emission with a second, high power, laser beam that is collinear with the excitation beam. This depletion beam is contrived to present approximately zero intensity on the optical axis but sufficiently high intensity elsewhere to fully deplete the excited fluorophore population. Typically, such depletion beams are formed by

Mark A. A. Neil, Christopher Dunsby and Paul M. W. French contributed equally to this study.

This is an open access article under the terms of the Creative Commons Attribution License, which permits use, distribution and reproduction in any medium, provided the original work is properly cited.

© 2018 The Authors. *Journal of Biophotonics* published by WILEY-VCH Verlag GmbH & Co. KGaA, Weinheim

propagating a laser beam at a wavelength that overlaps the fluorophore emission spectrum through a suitable phase retarding plate [2] to impart a helical phase profile in the back focal plane of the objective lens and hence achieve a so called “doughnut-shaped” PSF at the focus of the objective lens. [2] Alternatively, the required phase profile can be imparted using a spatial light modulator (SLM) [4, 5] that may also be used to correct for optical aberrations in the instrument [5] or sample. [6–8] More complex configurations can utilize multiple phase plates [9] or a multipassed SLM [8] to also shape the depletion beam intensity along the optical axis to provide axial super resolution. The achievable spatial resolution of RESOLFT approaches is fundamentally limited only by the available power in the photoswitching beam and, for STED microscopy, resolutions down to ~6 nm [10] have been achieved when imaging NV centers in polycrystalline CVD diamond. In biological samples, depletion powers are practically limited by the photostability of the sample and lateral resolutions in the ~30 to 100 nm range are more typical.

To achieve the highest spatial resolution for STED microscopy, the optimum phase profile should be imparted on the depletion beam and it should be collinear with the excitation beam when incident at the sample. Typically, the excitation and depletion beams follow different paths and the overlapping of these beams before the objective lens is a critical adjustment that presents challenges in terms of alignment and stability. To address this, Reuss et al presented the concept of “easySTED” [11] where collinear excitation and depletion beams both propagate through a suitable birefringent element that imparts an appropriate phase profile to the depletion beam but not the excitation beam. Because the excitation and depletion beams can easily be made collinear, e.g. by coupling them into a single mode optical fiber, it is relatively easy to maintain the optimum alignment for STED microscopy or to recover it if the input laser beams drift with respect to one another. This elegant and simple approach is, however, limited to a specific pair of excitation and depletion wavelengths and the lack of an SLM means that electronically controlled correction of aberrations is not available. We here follow the concept of “easySTED” and present an analogous approach that includes an SLM, which can be programmed for a range of excitation and depletion wavelengths and can be used to correct aberrations. We show that this can be applied to correct chromatic aberration in the scanner and thereby significantly extend the field of view of the STED microscope, and we demonstrate how it can be adapted for parallelized multibeam STED microscopy.

2 | easySLM-STED

Our “easySLM-STED” set-up is depicted in Figure 1. Excitation is provided by a 485 nm gain-switched diode laser (LDH-D-C-485, PicoQuant, Berlin, Germany) that provides

picosecond pulses at a tunable repetition frequency. The depletion laser is a custom-built frequency-doubled, Raman-shifted fiber laser providing pulses of 100’s ps duration at a wavelength of 560 nm. [12] The temporal profile of the pulse and repetition rate can be adjusted, for example, to optimize performance with a specific fluorophore. The pulsed excitation and depletion lasers are synchronized and beams from each laser with orthogonal polarization states are coupled into a single-mode, polarization maintaining optical fiber. The delay between the depletion and excitation pulses is adjusted using an electrical delay box (Precision Programmable Delay Line, Kentech Instruments Ltd, Wallingford, UK). The collinear excitation and depletion laser beams are collimated after the optical fiber and directed onto one half of an SLM (X10468-04 LCOS-SLM, Hamamatsu, Hamamatsu City, Japan) at B1 where only the excitation beam is horizontally polarized such that it can be modulated by the SLM. The SLM is connected to a desktop computer as a second display and is configured to display a hologram that diffracts the first order of the excitation beam by a specific angle. As the beams propagate from B1 to B2, they double pass an achromatic quarter wave plate (QWP) such that, as described previously for a 3-D STED microscope [8], their polarizations are rotated by $\pi/2$ radians and therefore at B2 only the depletion beam is modulated by the SLM, which is set to impart the helical phase profile required to form the “doughnut-shaped” depletion beam in the focal plane of the objective lens. The first order excitation beam diffracted from the SLM at B1 (with a different wavelength to the depletion beam) is set to diffract at the same angle as the first order depletion beam diffracted from the SLM at B2 such that the beams are collinear after the second interaction with the SLM at location B2. The collinear diffracted beams are eventually passed through a QWP that converts them to circular polarization states that are optimal for STED microscopy.

The collinear excitation and depletion beams are then relayed to a galvanometric scan unit (Yanus IV digital scan head, FEI, Munich, Germany) via a $\times 1.5$ expanding telescope and reflected off a dichroic beamsplitter (zt488/561rpc, Chroma, Vermont, USA) that separates the excitation and depletion beam from the fluorescence signal. After the scanner, the excitation and depletion beams are relayed to the 100x objective lens (HCX PLA APO 100 \times 1.4, Leica, Wetzlar, Germany) by a $\times 5$ magnification telescope formed by the 50 mm focal length scan lens and a 250 mm focal length achromat doublet lens (AC508-250-AML, Thorlabs, Newton, Massachusetts) that serves as the tube lens. The emitted fluorescence is relayed back through the scanner and transmitted through the dichroic beamsplitter for confocal detection using a graded index multimode optical fiber (M31L03, Thorlabs, Newton, Massachusetts) with a core size of 62.5 μm that serves as the pinhole. For adjustment purposes with scattering samples, a removable pellicle beamsplitter (pellicle bs) deflects some of the scattered signal to a larger multimode optical fiber of 1 mm core

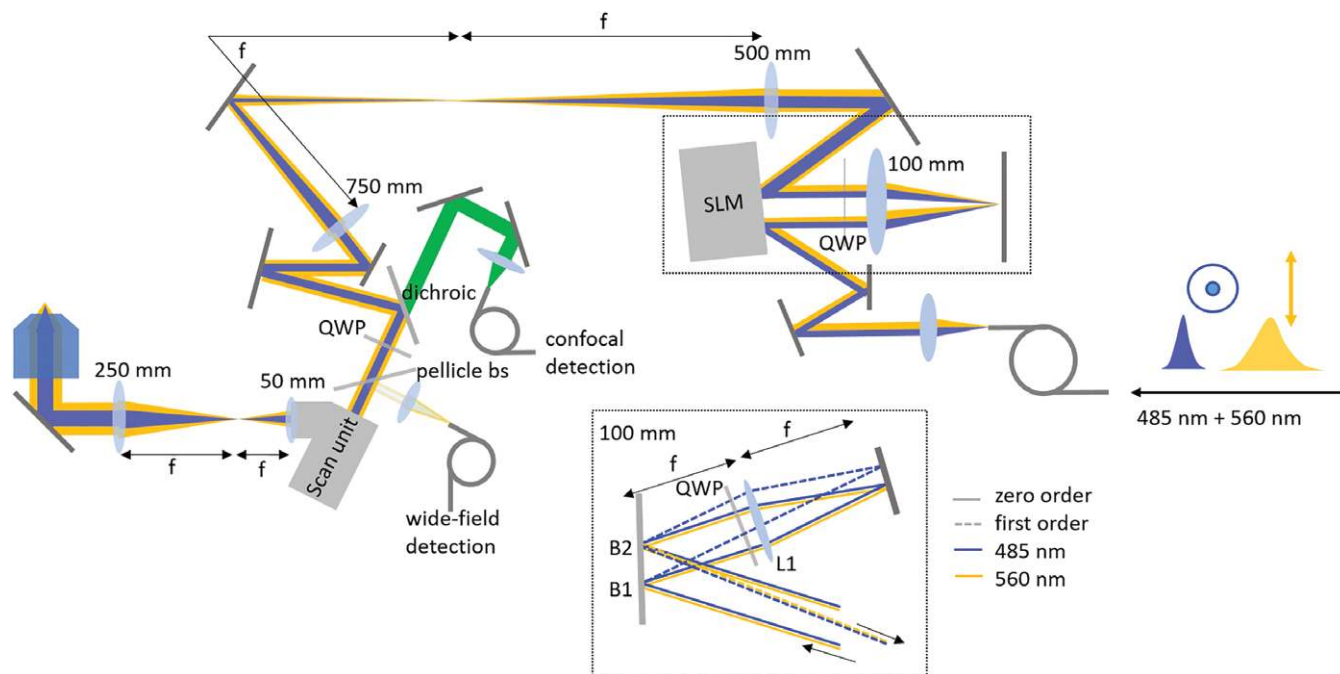


FIGURE 1 easySLM-STED set-up with inset of beam paths at the SLM: Excitation (485 nm) and depletion (560 nm) laser beams are collinear (drawn side by side for visualization) leaving the optical fiber (485 and 560 nm) with orthogonal polarizations. At location B1 on the SLM, the excitation beam is deflected to overlap the depletion beam in the imaging plane; a double pass through a quarter wave plate (QWP) rotates the polarization states of each beam by $\sim\pi/2$ radians and so at B2 the SLM modulates the depletion beam, imparting the helical phase profile. The excitation and STED beams then propagate collinearly via a dichroic beamsplitter that reflects them into a galvanometric scanner from where they are directed to the objective lens. The descanned fluorescence signal is transmitted through the dichroic beamsplitter to an optical fiber that serves as the aperture for confocal detection. N.B. the layout of the SLM is shown schematically in the main figure and the optical configuration is shown in the inset

diameter for wide-field detection. The fluorescence is detected using a hybrid PMT (HPM-100-40, Hamamatsu, Hamamatsu City, Japan), the electronic output of which could be connected to a DAQ box (NI USB-6259, National Instruments) after passing a constant fraction discriminator (TB-01, Horiba Scientific, Kyoto, Japan) or a time-correlated single photon counting (TCSPC) card (SPC-830, Becker & Hickl, Berlin, Germany) for time-integrated or time-resolved detection, respectively. The sample can be moved in all three dimensions using a x-y-z stage (NanoPDQ375HS, MCL Inc, Madison, Wisconsin). The instrumentation was controlled with an in-house LabVIEW program, with the images being acquired with the software package SPCM (Becker & Hickel, Berlin, Germany) and analysed with SPCImage (Becker & Hickl, Berlin, Germany) to apply time gating.

Figure 2 shows a typical easySLM-STED image of 46 nm diameter fluorescent beads (yellow-green beads, Invitrogen, Carlsbad, California), for which the field of view (FOV) is $10 \times 10 \mu\text{m}$ with a pixel size of 15 nm, recorded with a pixel dwell time of 100 μs , average excitation power of 12 μW (measured at the sample plane) and a corresponding average depletion power of 22 mW with pulses of 1.3 ns at 5 MHz repetition rate. This data was analysed using the ThunderSTORM [13] software package, which is typically employed to analyse single molecule localization microscopy (SMLM) data, and the 100 beads with the lowest FWHM (approximately half of the beads in the field of view) present a mean FWHM of 49 nm (STD of 7.54 nm).

Figure 3 shows confocal and easySLM-STED images of a Vero cell where vimentin is labeled with AbberiorSTAR-488 (Abberior GmbH, Göttingen, Germany). A $20 \times 20 \mu\text{m}$ FOV size was imaged with a pixel dwell time of 100 μs and a pixel size of 25 nm, accumulating 5 frames per image acquisition. The excitation and depletion laser pulse repetition rates were 5 MHz with average excitation and depletion powers of 8 μW and 2.5 mW respectively. Features down to 51 nm could be resolved, as illustrated in line scans in Figure S1 in Appendix S1.

Figure 4 shows the application of easySLM-STED to image meiotic chromosomes in from *Caenorhabditis elegans* nematodes expressing the axial element component HTP1 labelled with GFP [14]. During meiotic prophase, homologous chromosomes undergo a pairing process that culminates with the intimate alignment of homologous axial elements containing HTP1 at a distance of about 100 nm [15]. HTP1-GFP was labelled with Alexa-488 through the use of a GFP antibody (GFP Tag Polyclonal Antibody Alexa Fluor 488, Thermo Fisher, Waltham, Massachusetts). The *C. elegans germlines* were fixed, and stained as described in [14] before adding SlowFade Diamond mounting media (Thermo Fisher Scientific, Waltham, Massachusetts). The pixel dwell time was 100 μs with 3 frame accumulations and a pixel size of 30 nm. The excitation beam average power was 7 μW , the depletion beam average power was 3 mW and time gating was applied. In the easySLM-STED image

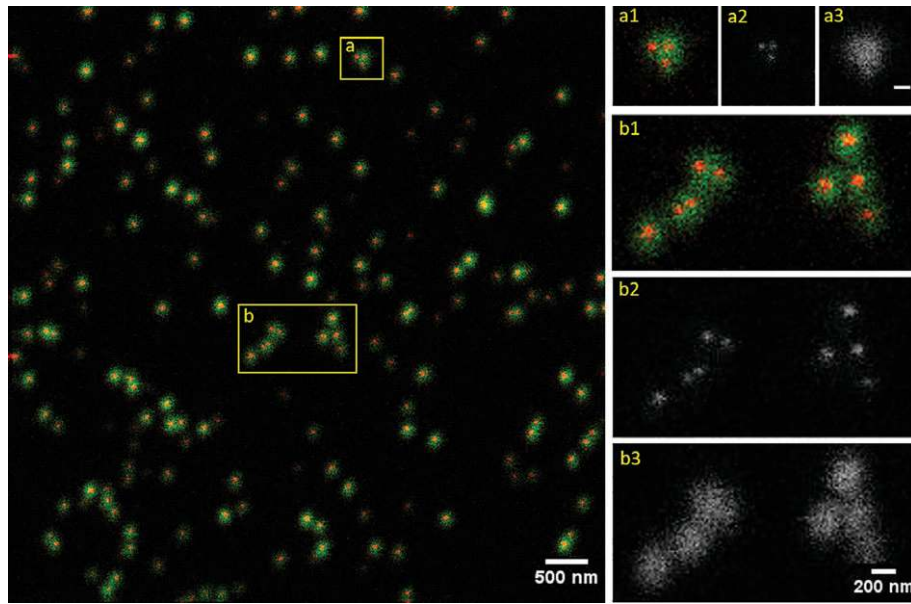


FIGURE 2 Main panel shows overlay of confocal (green) and easySLM-STED (red) images of 46 nm diameter fluorescent beads, that is acquired with and without the depletion beam; regions of interest (A, B) are shown with overlay (a1, b1) and with the corresponding STED (a2, b2) and confocal (a3, b3) images shown separately

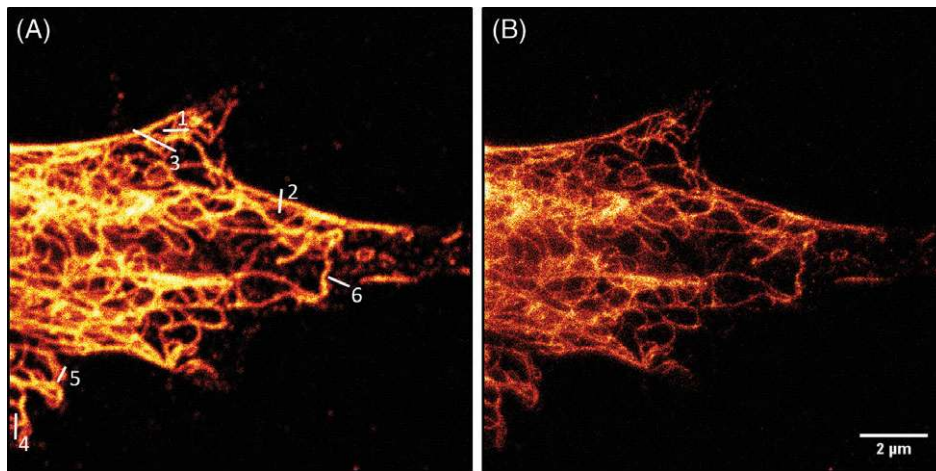


FIGURE 3 Confocal (A) and easySLM-STED (B) images of vimentin stained with AberriorSTAR-488 in a Vero cell. See Figure S1 in Appendix S1 for line scans

of Figure 4B, it is possible to resolve aligned axial elements from homologous chromosomes, which are not resolved in the corresponding confocal image of Figure 4A.

3 | CORRECTING CHROMATIC ABERRATION TO EXTEND THE STED FIELD OF VIEW

The use of two spatially separate regions on the SLM to control the excitation and depletion beams enables different phase modulations to be applied to the excitation and depletion beams. As well as generating the appropriate phase profiles to generate the required doughnut profile for the depletion beam, this approach can also be adapted to correct

for lateral chromatic aberration in the scanner and/or illumination optics that can lead to walk-off between the excitation and depletion beams as they are scanned further from the optical axis. Chromatic aberration is a well-known problem for multicolor confocal microscopy [16, 17], particularly for home-built microscopes that use stock combinations of tube lens and objective lenses.

This problem is particularly important for STED microscopy where the excitation and depletion beams inherently are at different wavelengths, which can make it challenging to maintain their overlap with sub-diffraction limited accuracy. The off-axis displacement between the excitation (green) and depletion (red) beams is illustrated in Figure 5, which shows representative images formed by light scattered from 80 nm diameter gold beads. A field of view of $100 \times$

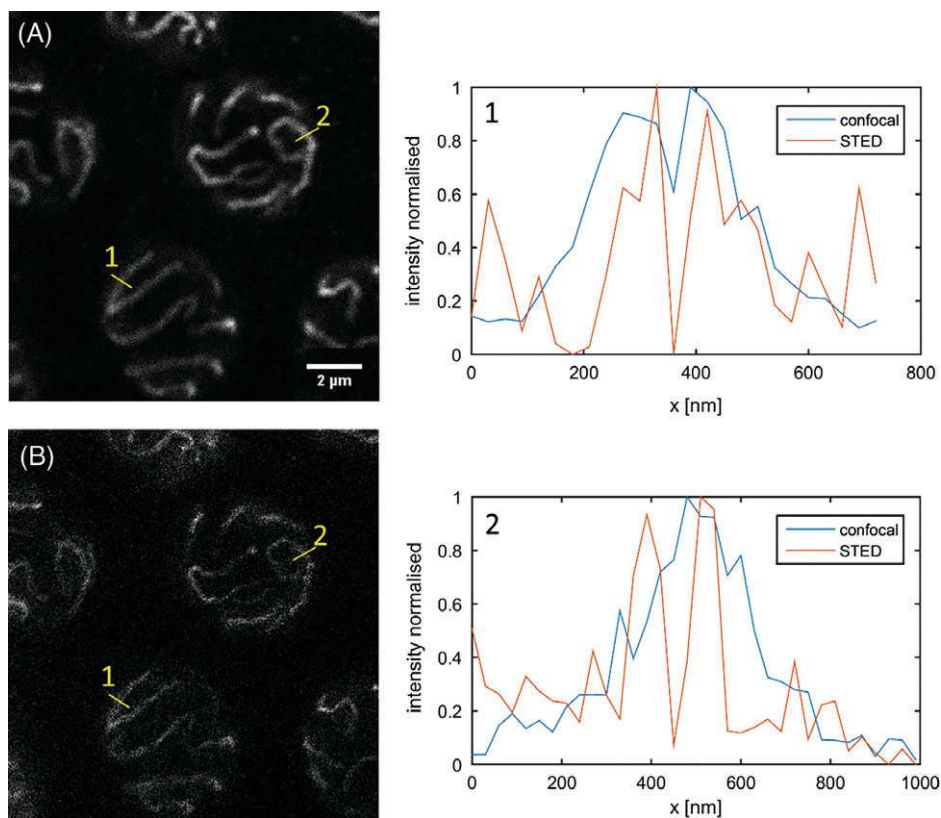


FIGURE 4 Confocal (A) and easySLM-STED (B) images of pachytene nuclei from a *Caenorhabditis elegans* germline in which the paired axial elements of each pair of homologous chromosomes was visualized by labelling the HTP-1 protein with Alexa-488. Axial elements from paired homologous chromosomes are clearly resolved in the STED, but not confocal, images as illustrated by the minima in the line profiles between the central peaks

100 μm was imaged and the tiles in the figure show $2 \times 2 \mu\text{m}$ subregions from within the entire FOV. The center of each tile with respect to the center of the entire field of view is shown at the bottom of each tile. Figure 5A shows the images obtained with no correction of the chromatic aberration and the walk-off of the excitation and depletion beams away from the optic axis of the objective lens is evident. Figure 5B shows the corresponding images when the SLM is used to apply a specific correction for the chromatic aberration for each image tile. The corrected images clearly show the advantage of this approach, with the excitation and depletion images remaining overlapped over the whole of the extended FOV. In principle, this approach can be adapted to correct for aberrations (and therefore extend the FOV) with almost any scanner used in a STED microscope.

To illustrate the performance of this aberration-corrected mosaic approach to extended FOV STED microscopy, a sample of 46 nm fluorescence beads was imaged with and without the chromatic aberration correction applied. A slight tilt of the coverslip of 400 nm over the diagonal of the FOV required the sample to be moved in the axial direction using the sample stage in order to image all these tiles. Also, it was observed that at large scan angles the fluorescence signal walked off the 0.74 Airy “pinhole” used to implement confocal sectioning (ie, the multimode optical fiber). This was corrected by appropriately changing the carrier frequency of both the excitation and depletion holograms to

shift them laterally by an equal amount. Figure 6A shows five $9 \times 9 \mu\text{m}$ STED image tiles of the 46 nm diameter fluorescent bead sample taken from the middle and the edges of the extended $100 \times 100 \mu\text{m}$ field of view. The total acquisition time to acquire the STED images of the 5×5 tiles, each $20 \times 20 \mu\text{m}$, was approximately 80 minutes. In Figure 6A the uncorrected images show that the image resolution is degraded in the corner tiles compared to the center tile. When the depletion PSF is no longer overlapping the excitation beam, the resolution is essentially that of the confocal microscope. However, the image quality will be degraded with respect to a confocal microscope image in regions where the walk-off of the fluorescence signal results in the lobes of the depletion PSF overlapping with the center of the excitation beam, giving unwanted depletion. Further image degradation will be seen at large scan angles where the chromatic aberration causes the fluorescence to walk off the confocal detection pinhole. In contrast, Figure 6B displays the corrected easySLM-STED image with homogenous resolution and signal to noise ratio across the extended FOV.

To further illustrate the efficacy of our correction procedures for easySLM-STED of large FOV, Figure 7 presents results from an analysis of the STED images using ThunderSTORM. Each dot on the image represents a bead identified by the software with the fitted FWHM being color-coded on the scale ranging from 0 nm (blue) to 250 nm (red). This therefore maps the variation in resolution achieved across

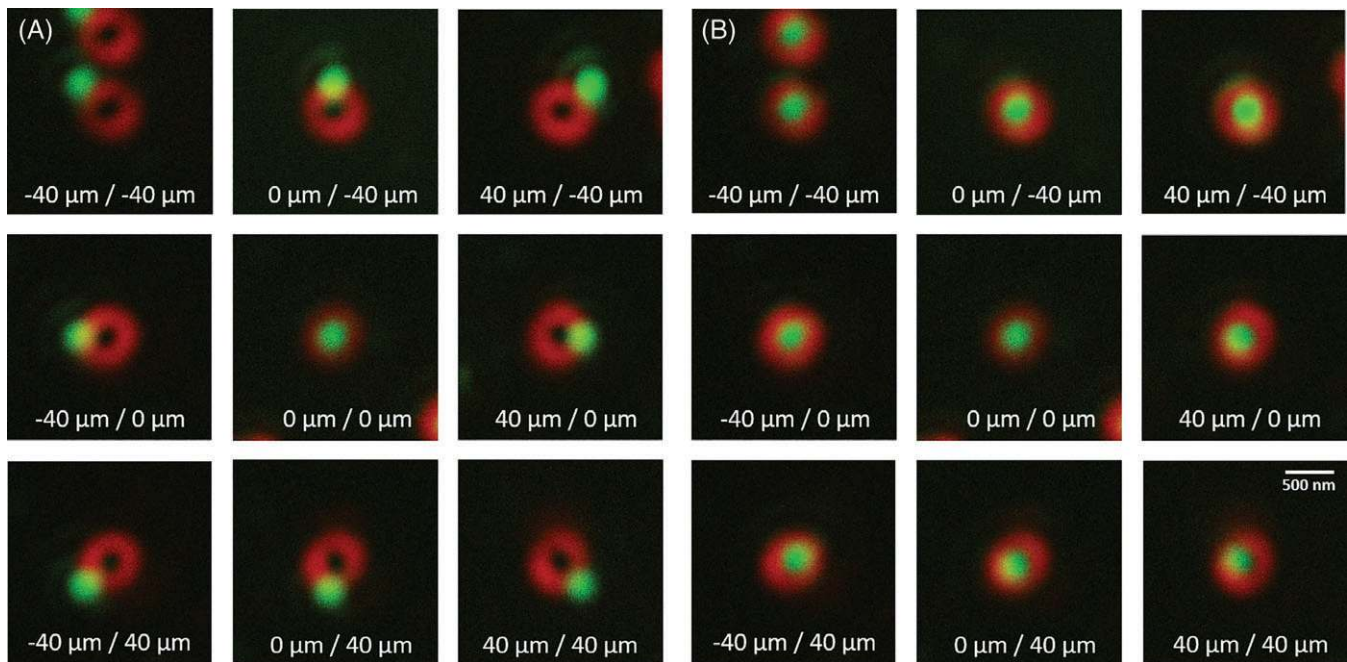


FIGURE 5 Images of light scattered from 80 nm diameter gold beads were acquired with wide-field detection over a FOV of $100 \times 100 \mu\text{m}$. Tiles of subregions within this FOV are shown without (A) and with (B) SLM correction of lateral and z-stage correction of axial chromatic aberration. The x/y coordinates of the center of each tile relative to the center of the entire FOV are given at the bottom of each tile

the extended FOV due to the various different beam paths through the scanning optics, tube lens and objective lens. The uncorrected STED data of Figure 7A shows a strong radial dependence of the resolution, which worsens from the center, degrading dramatically for radial distances of $\sim 25 \mu\text{m}$, at which point the excitation spot overlays the ring of the depletion doughnut and therefore the fluorescence signal is suppressed – resulting in a significant loss of bead localizations. As the radial distance from the optical axis passes $40 \mu\text{m}$, the excitation spot no longer overlaps the depletion ring and the resolution becomes the same as a confocal microscope. In contrast, Figure 7B displays the

corrected STED approach with a homogenous resolution far below the diffraction limit across the extended FOV.

The radial dependence of the resolution (calculated using ThunderSTORM) can be seen in Figure 8, which displays the FWHM (a) and bead intensity (b) as a function of the distance to the optical axis for easySLM-STED images acquired with (orange) and without (blue) the correction of aberrations across the extended FOV. The corrected STED resolution and bead intensity (as reported by ThunderSTORM integrating photon counts over each bead) are reasonably constant across the FOV, whereas the FWHM starts to increase linearly from 25 to $40 \mu\text{m}$

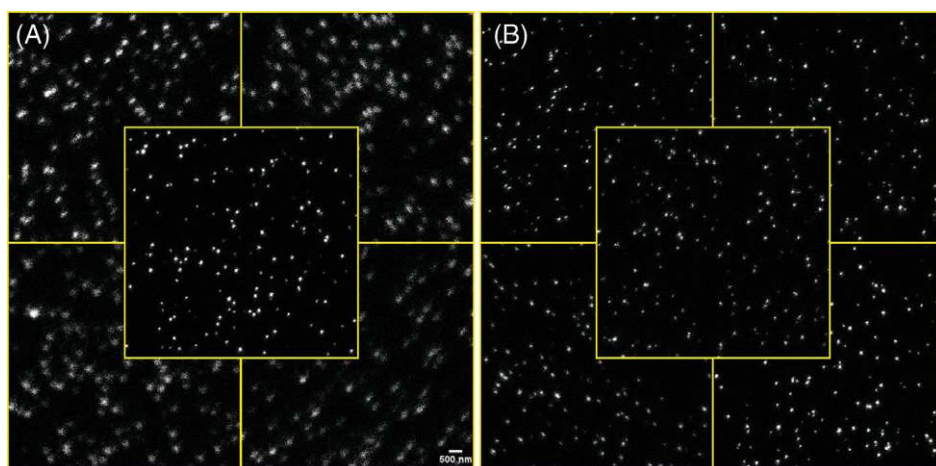


FIGURE 6 easySLM-STED image tiles of 46 nm diameter fluorescent beads taken from the corners and center of a $100 \times 100 \mu\text{m}$ FOV image where the images of (A) have been acquired with no correction of aberrations and (B) have had the corrections applied during the image acquisition

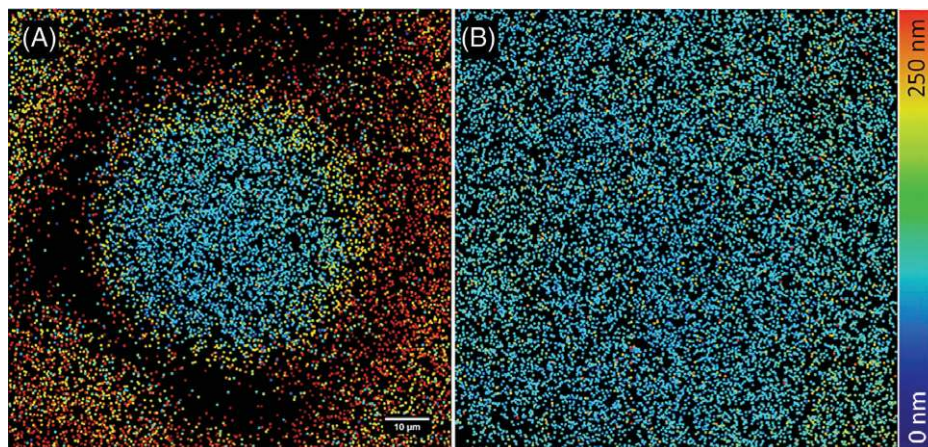


FIGURE 7 Measured lateral (FWHM) resolution across the extended $100 \times 100 \mu\text{m}$ FOV obtained using the easySLM-STED set-up where (A) has been acquired with no correction of aberrations and (B) has had the corrections applied during the image acquisition

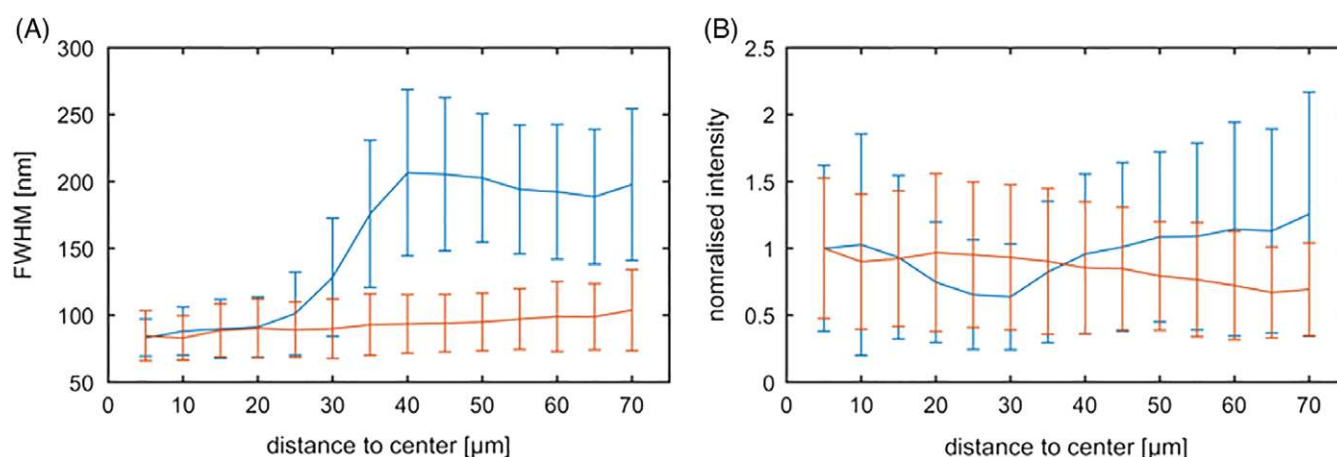


FIGURE 8 (A) FWHM of beads in Figure 7 as a function of radial distance of bead from the center of the FOV for the uncorrected (blue) and corrected (red) cases. (B) integrated bead intensity for the corrected (red) and uncorrected (blue) approaches as a function of radial distance of bead from center of the FOV

from the optical axis and then plateaus at the confocal resolution for the uncorrected case. The right graph shows the integrated localized bead intensity dependence on the radial distance from the optical axis with the localizations for the corrected STED remaining approximately constant until the edge of the FOV of $100 \times 100 \mu\text{m}$ is reached. For the uncorrected STED images, a dip can be observed around $25 \mu\text{m}$, where the excitation beam overlaps the ring of the depletion donut, after which the fluorescence is no longer significantly depleted, and the confocal resolution is reached.

This aberration-corrected mosaic implementation of easySLM-STED was also applied to fixed Vero cells in which the vimentin was labelled with AbberiorSTAR-488 (Abberior GmbH, Göttingen, Germany). Figure 9 shows confocal and STED images of a $100 \times 100 \mu\text{m}$ extended FOV, with selected regions of interest expanded and shown with corresponding line-scans to illustrate the improved resolution across this extended FOV. The image was divided into 5×5 tiles, each $20 \times 20 \mu\text{m}$, and the complete image was acquired in approximately 30 minutes.

4 | MULTIBEAM EASYSLM-STED MICROSCOPY TO IMPROVE THE ACQUISITION SPEED

The spatial modulation of excitation and depletion laser beam in the easySLM-STED approach can be extended to implement parallelized super resolution microscopy in order to increase the image acquisition speed. Parallelized STED microscopy was previously been demonstrated using four pairs of excitation and depletion beams [18] utilizing polarization multiplexing. This was increased to an optical lattice of up to 100 depletion minima formed by multibeam interference applied with wide-field excitation [19] and later to >2000 depletion minima [20], with both approaches using camera-based detection. We were interested to develop a set-up that could generate an arbitrary number of excitation/depletion beam pairs and here present an implementation of a $4\times$ parallelization of STED microscopy in conjunction with photomultiplier (PMT) detection, which enables time-resolved measurements for fluorescence lifetime imaging and/or gating of super-resolved fluorescence [5].

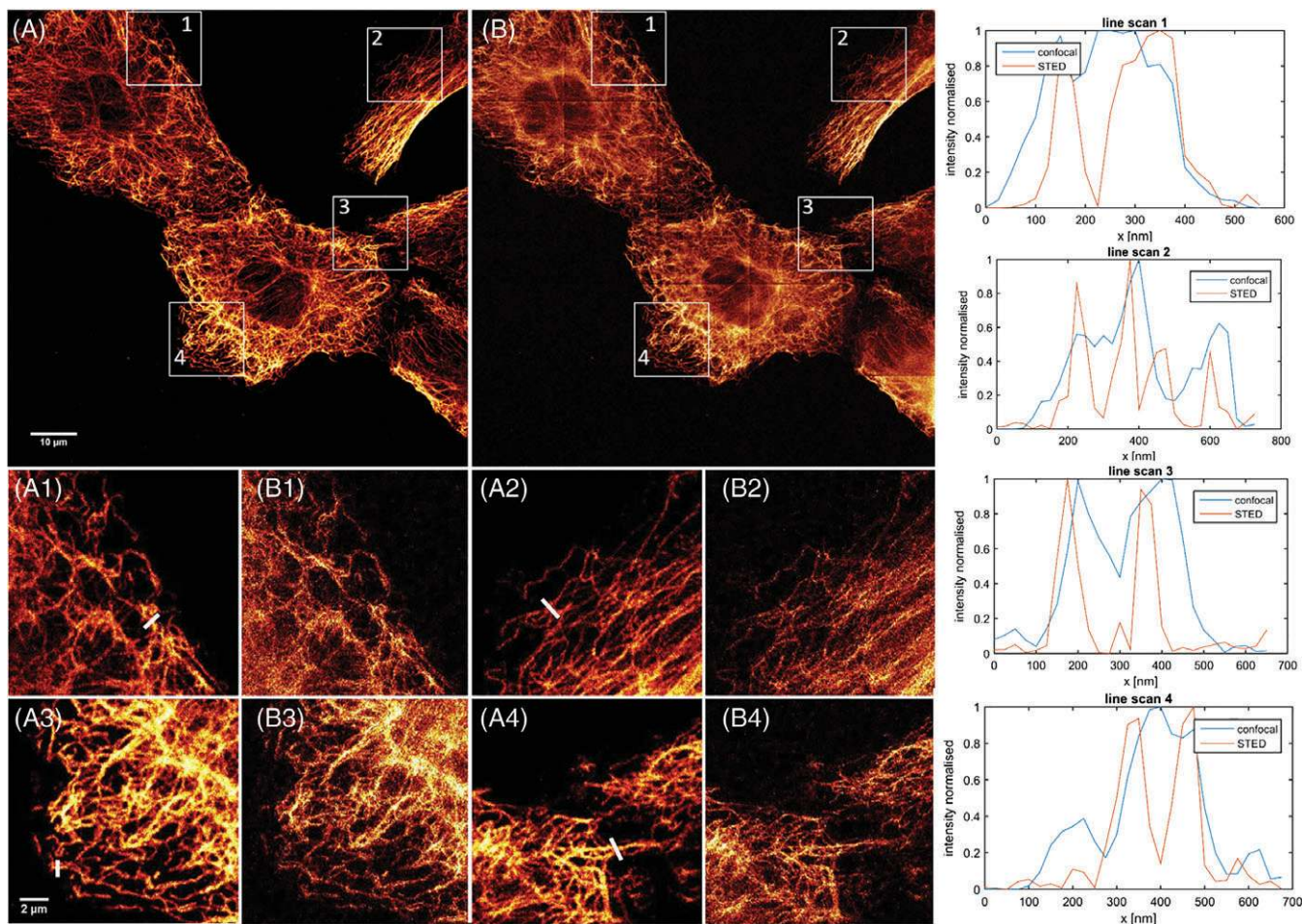


FIGURE 9 Confocal (A) and easySLM-STED (B) mosaic images of $100 \times 100 \mu\text{m}$ extended FOV of vimentin labelled with AbberiorSTAR-488 in fixed Vero cells with expanded images and corresponding line scans of subregions of (A, B) as indicated

The holograms written to the SLM can be programmed to diffract an arbitrary number of beams for each incident beam and here the SLM is set to produce four excitation and depletion beams arranged in a line. The double pass implementation of the SLM enabled holograms to be applied to result in four excitation PSFs overlaid with four depletion doughnuts, as represented in Figure 10. The required holograms were calculated iteratively using an inverse approach for which the desired target intensity distribution in the sample plane is defined and then a random phase is applied to the hologram, with its Fourier transformation (which corresponds to the diffracted output beams) being compared with the defined target distribution. The phase of each pixel in the hologram is adjusted in turn to reduce the difference between the actual and the desired target distribution until a minimum is reached. Further information about this process is given in the Appendix S1, Supplementary Information. This program was written in MATLAB and a C MATLAB executable was generated, which could be called by the LabVIEW program that controlled the instrument. Here we implemented the generation of up to 4 parallel excitation/depletion beams that could be programmed to place the PSFs across the focal plane, and 2D astigmatism correction was implemented. In principle, this approach could be extended to more parallel beams and more

complex aberration corrections could be applied. For parallel detection, the fluorescence PSFs were imaged onto a linear array of multimode fibers (M31L03, Thorlabs, fixed in place with Epoxy F112, Thorlabs, Newton, Massachusetts). The outputs of the optical fibers were coupled to four PMTs (H7422P, Hamamatsu, Hamamatsu City, Japan) and the resulting electrical signals were connected to a TCSPC card (SPC-830, Becker & Hickel, Berlin, Germany) via a router (HRT-41, Becker & Hickel, Berlin, Germany).

A four times speed improvement was demonstrated by imaging 46 nm fluorescence beads and the imaging performance was comparable to that achieved when using a single scanning excitation/depletion beam pair, as shown in Figure 11. Here, a $10 \times 10 \mu\text{m}$ FOV was imaged with the single scanning excitation/depletion beam pair and with four parallel beam pairs, each scanning a $2.5 \times 10 \mu\text{m}$ sub-FOVs, which reduced the image acquisition time from 48 to 12 seconds. The resolution in all four channels is similar, with a mean FWHM of 61 nm (SD 17 nm) for the 4x parallel imaging and 65 nm (SD 24 nm) obtained with the single scanning beam pair. These results are summarised in Table S1 in Appendix S1. The pixel size was 25 nm and images were acquired with an integration time of 300 μs /pixel. The excitation power measured at the

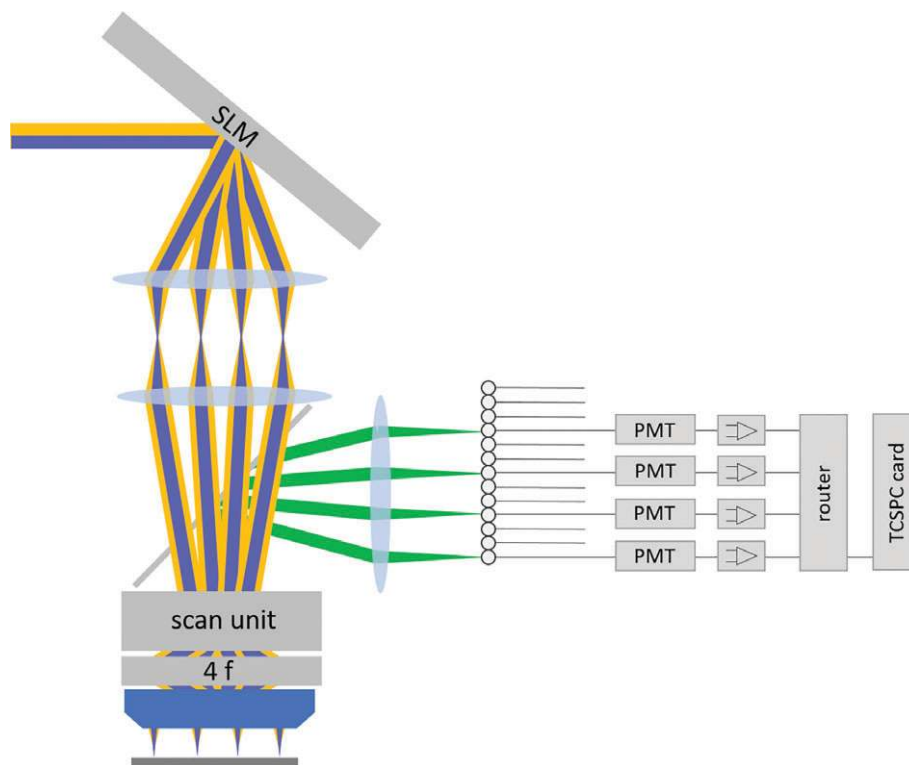


FIGURE 10 Simplified schematic of the optical configuration for multibeam easySLM STED. The collimated collinear excitation and depletion beams incident at the SLM are diffracted in the double pass arrangement of the SLM in the same way as for the single beam pair, but the holograms written to the SLM are programmed to diffract four beams at B1 and B2 such that four excitation/depletion beam pairs emerge from the second pass of the SLM. These are relayed to the scan unit and onto the sample where the four beam pairs are focused to acquire STED image data from four locations in parallel. The fluorescence from the four excited/depleted foci is imaged to an array of optical fibers that serve as confocal detection pinholes and the light from each fiber is detected using a single photon counting photomultiplier. The electrical signals from the four photomultipliers are combined using an electronic router and fed to a TCSPC card

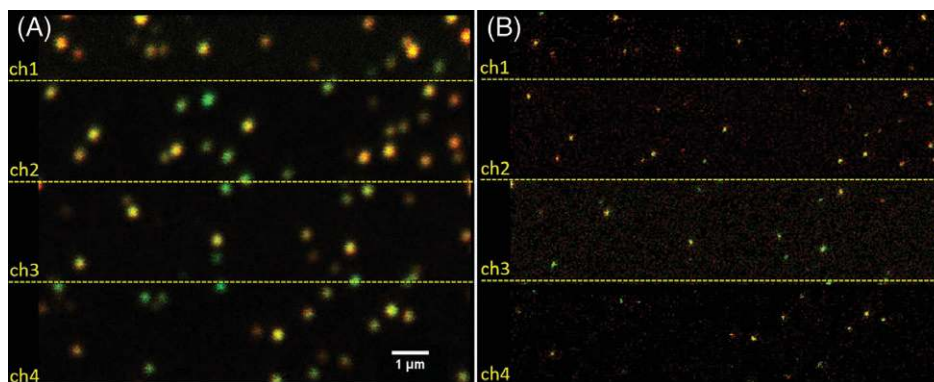


FIGURE 11 Multibeam easySLM-STED images of field of view of fluorescent beads. (A) confocal image acquired with single scanning beam pair (red) and four scanning beam pairs (green), (B) corresponding easySLM-STED images. Note that the images are adjusted such that the centers of the brightest beads saturate the image in order that more of the dimmer beads can be seen

microscope objective back aperture was maintained at $\sim 8 \mu\text{W}$ per beam and the depletion power at $\sim 7 \text{ mW}$ per beam for both single and four channel imaging. For this data set, the multibeam scanned images were acquired before the single beam scanned images and some of the beads were significantly photobleached by the second confocal and STED acquisitions such that they appear green in the color overlay.

We also applied this multibeam easySLM-STED microscope to image the axial elements of meiotic chromosomes

from *C. elegans* as discussed above. Again, the aligned (at a distance of about 100 nm) axial elements from homologous chromosomes could be resolved, as shown in Figure 12, with the 4 \times multibeam parallelization reducing the image acquisition time from 48 to 12 seconds. The pixel size was 25 nm with a pixel dwell time of 100 μs using 3 frame accumulations. The image size was $10 \times 10 \mu\text{m}$ or $4 \times 2.5 \mu\text{m} \times 10 \mu\text{m}$. The excitation and depletion powers per beam were $7.8 \mu\text{W}$ and 3 mW at the microscope objective back aperture, respectively.

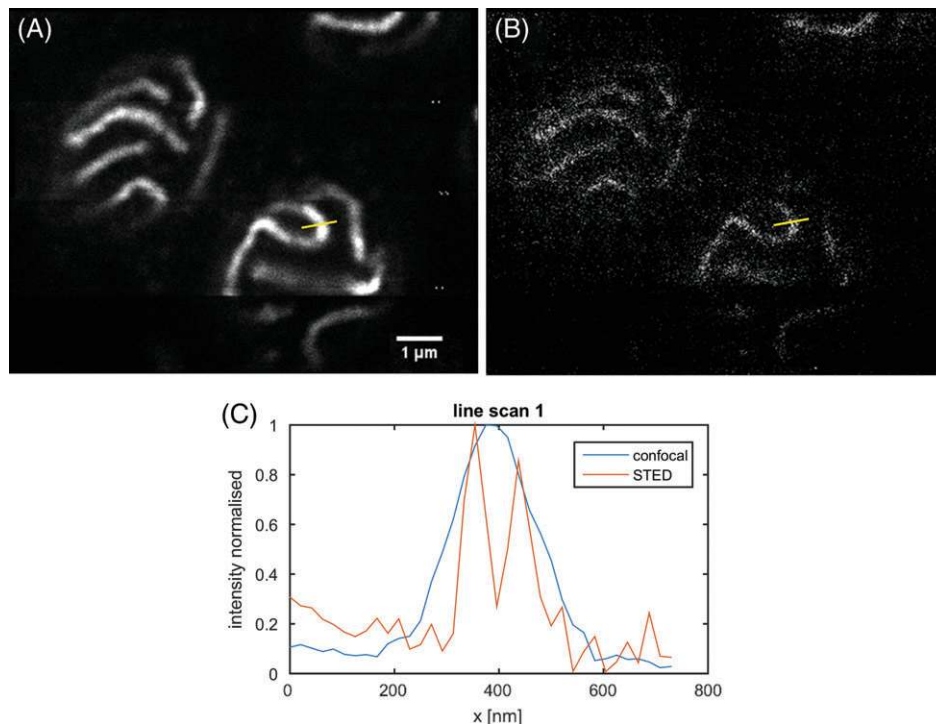


FIGURE 12 Multibeam easySLM-STED image of pachytene nuclei from *Caenorhabditis elegans* expressing HTP1-GFP labelled with Alexa-488 to visualize the axial elements from homologous chromosomes (A) 4× multibeam confocal scan, (B) 4× multibeam STED and (C) corresponding line-scans.). Note that homologous axial elements are only resolved in the STED image

5 | CONCLUSIONS

We have demonstrated a robust set-up for STED microscopy that uses a single spatial light modulator (SLM) with collinear incident excitation and depletion beams that can correct optical aberrations in both beams. As well as resulting in relatively straightforward alignment procedures for the laser beams, this approach enables the field of view for STED microscopy to be extended by correcting lateral chromatic aberration that otherwise leads to walk-off between the focused excitation and depletion beams with increasing distance from the optical axis. This therefore relaxes the requirements for scanners used in STED microscopy.

We have further shown how this arrangement can be adapted to increase the imaging speed through multibeam excitation and depletion. Although the alignment to multiple detection optical fibers is potentially challenging, we note that the SLM permits fine adjustments to the alignment to be accomplished electronically, conferring the potential for automation—which would also be the case with a single detector. Overall, we believe the easySLM-STED approach provides a reasonable balance between function (including aberration correction) and ease of set up and maintenance.

ACKNOWLEDGMENTS

The authors would like to acknowledge the expert help from Martin Kehoe, Simon Johnson and Jon Murphy in the Optics Workshop who particularly helped design and fabricate the

components for multibeam detection system. The authors gratefully acknowledge funding from the UK Medical Research Council (MRC, MR/K015834/1). F.G. acknowledges a PhD studentship from the Engineering and Physical Sciences Research Council. The raw image data underlying this publication is available from <https://omero.bioinformatics.ic.ac.uk/omero/webclient/?show=project-4753>.

ORCID

Frederik Görlitz  <http://orcid.org/0000-0002-8415-1820>

REFERENCES

- [1] S. W. Hell, J. Wichmann, *Opt. Lett.* **1994**, *19*, 780.
- [2] T. A. Klar, S. Jakobs, M. Dyba, A. Egner, S. W. Hell, *Proc. Natl. Acad. Sci. U.S.A.* **2000**, *97*, 8206.
- [3] M. Hofmann, C. Eggeling, S. Jakobs, S. W. Hell, *Proc. Natl. Acad. Sci. U.S.A.* **2005**, *102*, 17565.
- [4] G. Donnert, J. Keller, R. Meddam, M. A. Andrei, S. O. Rizzoli, R. Lührmann, R. Jahn, C. Eggeling, S. Hell, *Proc. Natl. Acad. Sci. U.S.A.* **2006**, *103*, 11440.
- [5] E. Auksoorius, B. R. Boruah, C. Dunsby, P. M. P. Lanigan, G. Kennedy, M. A. A. Neil, P. M. W. French, *Opt. Lett.* **2008**, *33*, 113.
- [6] E. B. Kromann, T. J. Gould, M. F. Juette, J. Wilhelm, J. Bewersdorf, *Opt. Lett.* **2012**, *37*, 1805.
- [7] T. J. Gould, D. Burke, J. Bewersdorf, M. J. Booth, *Opt. Express* **2012**, *20*, 20998.
- [8] M. O. Lenz, H. G. Sinclair, A. Savell, J. H. Clegg, A. C. N. Brown, D. M. Davis, C. Dunsby, M. A. A. Neil, P. M. W. French, *J. Biophotonics* **2014**, *7*, 29.
- [9] D. Wildanger, R. Medda, L. Kastrop, S. W. Hell, *J. Microsc.* **2009**, *236*, 35.
- [10] E. Rittweger, K. Y. Han, S. E. Irvine, C. Eggeling, S. Hell, *Nat. Phot.* **2009**, *3*, 144.
- [11] M. Reuss, J. Engelhardt, S. W. Hell, *Opt. Express* **2010**, *18*, 1049.

- [12] T. H. Runcorn, F. G. Görlitz, R. T. Murray, E. J. R. Kelleher, *IEEE J. Sel. Top. Q. Electron.* **2018**, *24*, 1.
- [13] M. Ovesný, P. Křížek, J. Borkovec, Z. Švindrych, G. M. Hagen, *Bioinformatics* **2014**, *30*, 2389.
- [14] E. Martinez-Perez, M. Schvarzstein, C. Barroso, J. Lightfoot, A. F. Dernburg, A. M. Villeneuve, *Genes Dev.* **2008**, *22*, 2886.
- [15] K. J. Hillers, V. Jantsch, E. Martinez-Perez, J. L. Yanowitz, WormBook, ed. The *C. elegans* Research Community, WormBook, The germ line - Judith Kimble and Susan Strome, eds. 2017, Meiosis, <http://www.wormbook.org/index.html>
- [16] W. J. Smith, *Practical Optical System Layout: And Use of Stock Lenses*, McGraw-Hill, New York **1997**.
- [17] A. Negrean, H. D. Mansvelder, *Biomed. Opt. Express* **2014**, *5*, 1588.
- [18] P. Bingen, M. Reuss, J. Engelhardt, S. W. Hell, *Opt. Express* **2011**, *19*, 23716.
- [19] B. Yang, F. Przybilla, M. Mestre, J. Trebbia, B. Lounis, *Opt. Express* **2014**, *22*, 5581.
- [20] F. Bergermann, L. Alber, S. J. Sahl, J. Engelhardt, S. W. Hell, *Opt. Express* **2015**, *23*, 211.
- [21] M. A. A. Neil, R. Juskaitis, T. Wilson, Z. J. Laczik, V. Sarafis, *Opt. Lett.* **2000**, *25*, 245.
- [22] M. A. Seldowitz, J. P. Allebach, D. W. Sweeney, *Appl. Optics* **1987**, *26*, 2788.
- [23] M. P. Dames, R. J. Dowling, P. McKee, D. Wood, *Appl. Optics* **1991**, *30*, 2685.

SUPPORTING INFORMATION

Additional supporting information may be found online in the Supporting Information section at the end of the article.

Appendix S1 Generation of holograms

FIGURE S1 Line scans as indicated in Figure 3

FIGURE S2 (A) Predicted intensity distributions of multiple focused beams in the sample plane together with the designed holograms. In each column there is: top, a Roman numeral indicating the number of doughnut-shaped intensity profiles to be generated; middle, the predicted intensity distribution; and bottom, the corresponding designed hologram. (B) Shows the experimentally measured intensity distributions shown with the same layout as for (A)

TABLE S1 FWHM, SD, intensity and number of beads found for each detection channel with average number (chAll) compared to a single beam scan for confocal and STED mode

How to cite this article: Görlitz F, Guldbrand S, Runcorn TH, et al. easySLM-STED: Stimulated emission depletion microscopy with aberration correction, extended field of view and multiple beam scanning. *J. Biophotonics*. 2018;e201800087. <https://doi.org/10.1002/jbio.201800087>